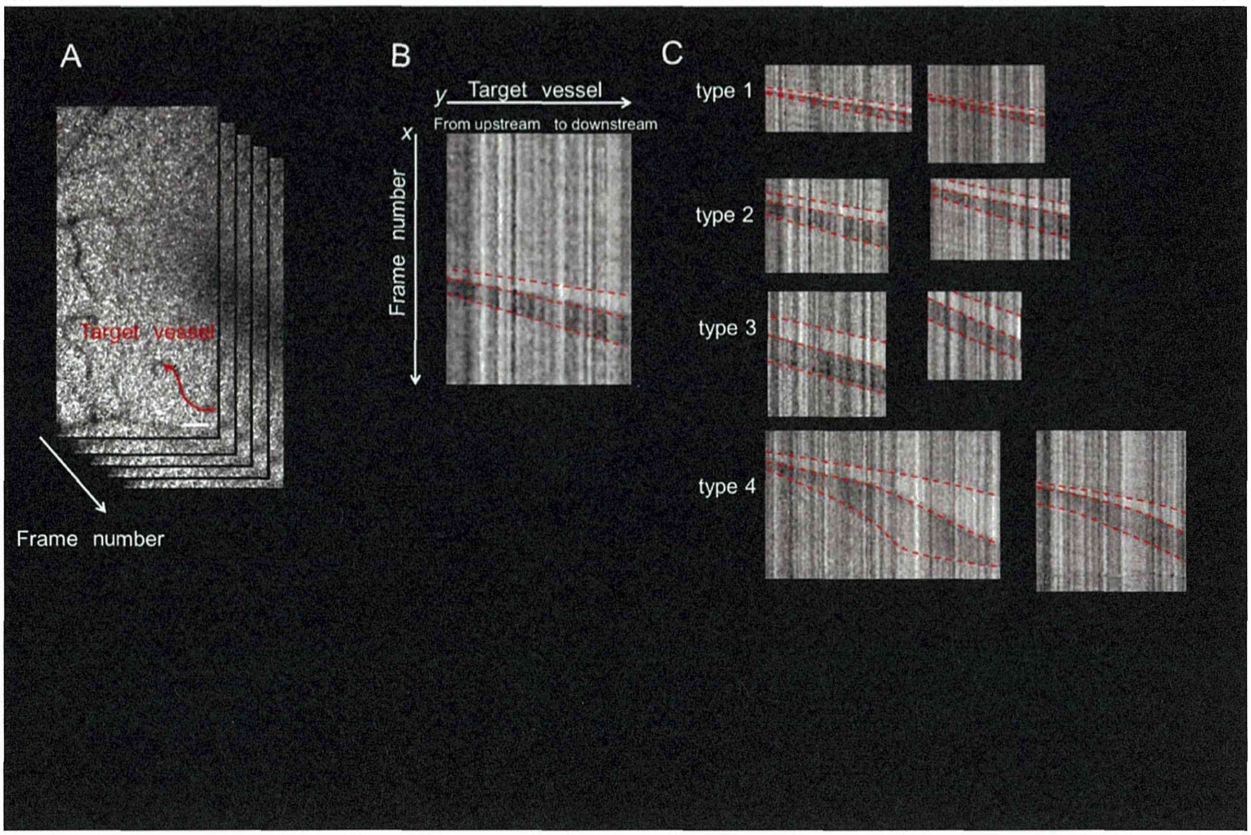

FIGURE 2. The characterization of STI images generated from AO-SLO videos of the parafoveal capillary network. (**A**) The target vessel on the consecutive frames of the AO-SLO. The *red line* represents the target vessel for analysis. *Scale bar*: 100 μm. (**B**) The ST image generated from the AO-SLO video by reslicing the frames along the line set on the target vessel. The white band paired with dark bands correspond to the trajectories of leukocytes (mainly) and erythrocyte aggregates, respectively. The *topmost red dashed line* represents the head of the white band. The *middle red dashed line* represents the border between the white and black bands, and the inverse of this slope corresponds to the head of erythrocyte aggregate velocity. The *bottommost red dashed line* represents the tail end of the black band. (**C**) The categorization of ST images into four types include the following: type 1, white and black bands widen gradually; type 2, white and black bands start out wider than type 1, then widen; type 3, both bands exhibit small changes in width; type 4, the slope of the bands bends concavely or convexly when traveling in a vessel free of bifurcations.

RESULTS

The characteristics of diabetic patients are listed in the Table. No significant difference was found in age among the groups ($P = 0.67$). The average axial lengths were 24.8 ± 1.2 mm in the normal group, 24.4 ± 0.9 mm in the NDR group, and 24.2 ± 1.1 mm in the NPDR group, with no significant difference among the groups ($P = 0.36$). The average HbA1c level was 9.1 ± 1.9 in the NDR group and 8.7 ± 1.8 in the NPDR group, with no significant difference between groups ($P = 0.95$).

Reproducibility of the Measurement of Velocity and Erythrocyte Aggregate Elongation Rate

The overall average velocities of five bins in five normal subjects were 1.25 ± 0.36 mm/s during the first measurement, 1.24 ± 0.38 mm/s during the second, and 1.34 ± 0.45 mm/s during the third ($P = 0.27$) (Supplementary Fig. S1). The total average erythrocyte elongation rate in five normal subjects was 0.85 ± 0.23 during the first measurement, 0.74 ± 0.12 during the second, and 0.94 ± 0.19 during the third ($P = 0.18$) (Supplementary Fig. S1). No significant difference was observed among the three velocity and erythrocyte aggregate elongation rate measurements.

Rapid Changes in Erythrocyte Aggregate Velocities in Diabetic Patients

In total, images of sufficient quality for the calculation of velocity were obtained for 768 erythrocyte aggregates from 20 (100%) normal subjects, 500 erythrocyte aggregates from 17 (100%) patients with NDR, and 173 erythrocyte aggregates from 10 (100%) patients with NPDR. Although all velocity calculations were performed relative to the cardiac cycle at average velocity, interestingly, one vessel with two erythrocyte aggregates from one (5.0%) normal subject, six vessels with nine erythrocyte aggregates from five (29.4%) patients with NDR, and six vessels with nine erythrocyte aggregates from five (50.0%) patients with NPDR showed rapid velocity changes in type 4 ST images, showing the bands bent concavely or convexly while traveling through a vessel free of bifurcations (Fig. 2; Supplementary Movie S2). These inconstant velocities were excluded from the analyses of average velocity, PI, and elongation rate.

Differences in Erythrocyte Aggregate Velocity Between Normal Subjects and Diabetic Patients

In the normal group, the overall average velocity of all five bins was 1.26 ± 0.22 mm/s; average velocities of individual bins

Investigative Ophthalmology & Visual Science

Downloaded From: http://iovs.arvojournals.org/pdfaccess.ashx?url=/data/Journals/IOVS/933678/ on 05/29/2015 Terms of Use:

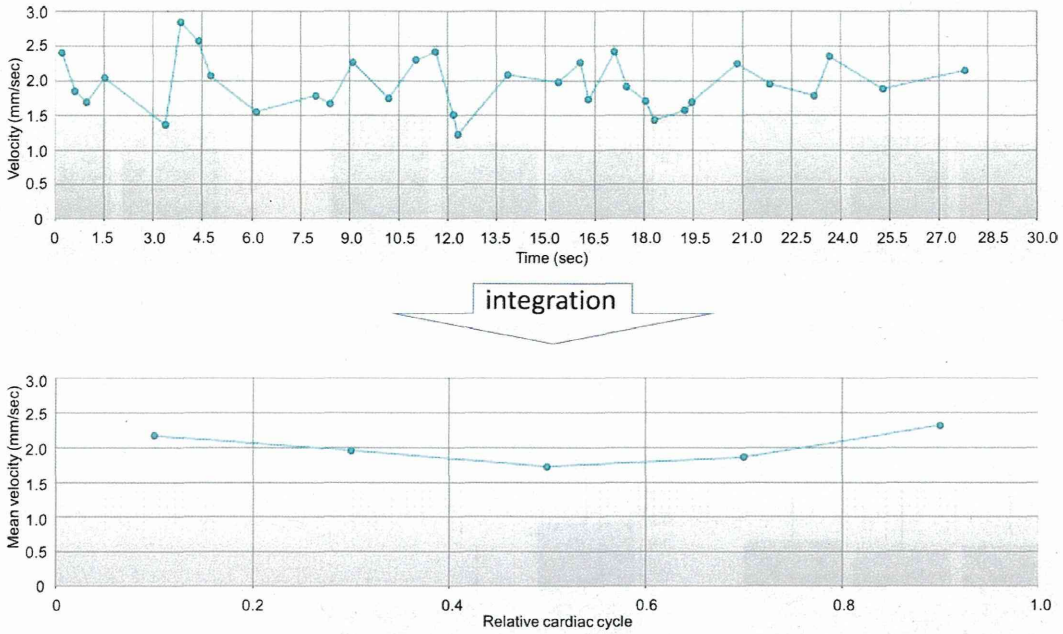

FIGURE 3. Velocity and cardiac pulsation synchronization. The sphygmogram was digitized and recorded during the imaging session. The AO-SLO image analysis software detected extreme values from the sphygmogram and then determined the relative cardiac cycle for each frame of the captured AO-SLO video. By dividing the relative cardiac cycle into 5 equal segments and averaging the raw velocities within each segment, mean erythrocyte aggregate velocity was plotted against relative cardiac cycle.

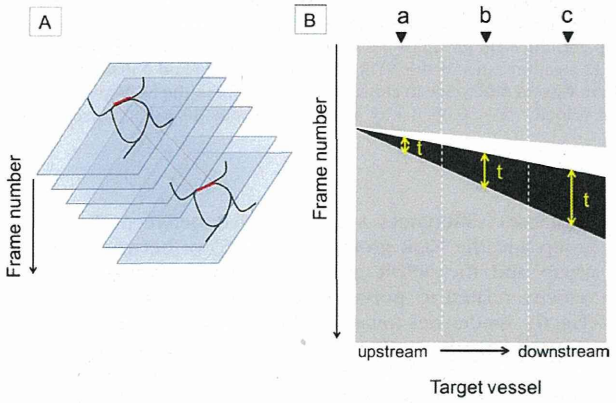

FIGURE 4. Measurement of erythrocyte aggregate velocity and length using spatiotemporal images. (**A**) Stacked sequential frames of the AO-SLO video. Frames are resliced along the *red line* set on the target vessel in order to generate the ST image. (**B**) Erythrocyte aggregate velocity and length were calculated using the ST image plotted with the length of the target vessel on the horizontal axis and the frame number on the vertical axis. The *white band* and the wider *black band* represent the trajectory of moving leukocytes (mostly) and erythrocyte aggregates, respectively. The thickness of the *black band* (t) represents the time required for the dark tail to pass through a point located on the target vessel. The reciprocal of the slope of the border between the *white* and *black bands* represents the velocity of the head of the erythrocyte aggregate. The ST image was vertically separated into three zones from upstream to downstream with respect to blood flow (zones a, b, and c). Erythrocyte aggregate length was calculated by multiplying the velocity by the time required to evaluate the elongation rate for each zone.

TABLE. Characteristics of Diabetic Patients

	Patients Without Diabetic Retinopathy	Patients With Nonproliferative Diabetic Retinopathy	*P* Value
Age, y	39.9 ± 11.7	39.9 ± 13.6	0.997
Sex (male/female)	9/8	6/4	
Diabetic type (type1/type2)	8/9	4/6	-
Stage of nonproliferative diabetic retinopathy			
Mild	NA	5	
Moderate	NA	5	
Severe	NA	0	-
HbA1c, %	9.1 ± 1.8	8.7 ± 1.8	0.606
Duration of diabetes, y	3.69 ± 3.47	14.8 ± 6.8	<0.0001
Medications			
Diet	1	0	
Insulin	11	4	
Oral	4	1	
Insulin and oral	1	5	-
Blood pressure, mm Hg			
Systolic	114 ± 15	124 ± 10	0.104
Diastolic	71 ± 14	77 ± 12	0.302
Intraocular pressure, mm Hg	14.2 ± 2.7	15.7 ± 2.6	0.179
Red blood cells, $\times 10^4/mm^3$	479 ± 44	492 ± 47	0.477
White blood cells, mm^3	6982 ± 2293	5699 ± 922	0.105

NA indicates not applicable.

Investigative Ophthalmology & Visual Science

Downloaded From: http://iovs.arvojournals.org/pdfaccess.ashx?url=/data/Journals/IOVS/933678/ on 05/29/2015 Terms of Use:

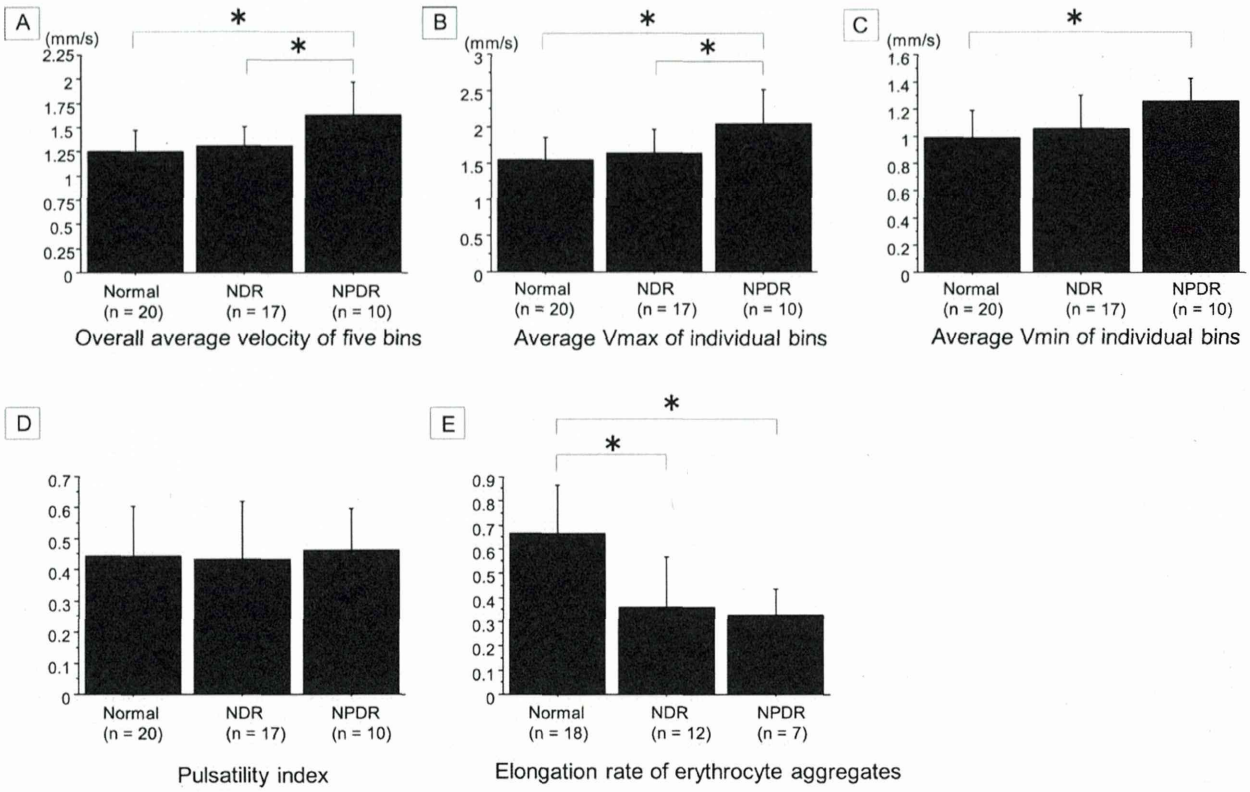

FIGURE 5. Comparison of erythrocyte aggregate velocity, elongation rate, and pulsatility index among normal subjects, patients without diabetic retinopathy, and patients with NPDR. (**A**) The overall averaged velocity for the 5 bins in the NPDR group was significantly higher than that of the normal group ($P = 0.001$) and the group without diabetic retinopathy (NDR) ($P = 0.009$). There were no significant differences between the normal group and the NDR group in overall average velocities. (**B**) The maximum velocities of individual bins in the NPDR group were significantly higher than those in the normal group ($P = 0.003$) and the NDR group ($P = 0.02$). Significant difference was not observed between the normal group and the NDR group. (**C**) The minimum velocities of individual bins in the NPDR group were significantly higher than those in the normal group ($P = 0.007$). No significant differences were observed between the normal group and the NDR group or between the NDR group and the NPDR group. (**D**) No significant differences in PI were detected among the groups. (**E**) Elongation rates in the NDR group ($P = 0.003$) and NPDR ($P = 0.001$) group were significantly lower than those in the normal group; however, there was no difference in elongation rate between the NDR group and the NPDR group ($P = 0.93$). V_{max} indicates maximum velocity; V_{min}, minimum velocity. *$P < 0.05$, 1-way ANOVA, with post hoc comparisons tested using the Scheffe test.

ranged from 1.04 to 1.45 mm/s, and individual erythrocyte aggregate velocities measured for all subjects ranged from 0.36 to 3.43 mm/s. In the NDR group, the overall average velocity of all five bins was 1.31 ± 0.21 mm/s; average velocities of individual bins ranged from 1.21 to 1.45 mm/s, and individual erythrocyte aggregate velocities measured for all subjects ranged from 0.46 to 4.01 mm/s. In the NPDR group, the overall average velocity of all five bins was 1.63 ± 0.35 mm/s; average velocities of individual bins ranged from 1.44 to 1.87 mm/s, and individual erythrocyte aggregate velocities measured for all subjects ranged from 0.71 to 4.19 mm/s (Supplementary Movie S3). There were no significant differences between the normal group and the NDR group in overall average velocity ($P = 0.789$) (Fig. 5A). The overall velocities in the NPDR group were significantly higher than those in the normal group ($P = 0.001$) and those in the NDR group ($P = 0.009$). The maximum velocities of individual bins in the NPDR group were significantly higher than those in the normal group ($P = 0.003$) and the NDR group ($P = 0.02$) (Fig. 5B). Significant difference was not observed between the normal group and the NDR group ($P = 0.77$). The minimum velocities of individual bins in the NPDR group were significantly higher than those in the normal group ($P = 0.007$) (Fig. 5C). No significant differences were observed between the normal group and the NDR group ($P = 0.585$) or between the NDR group and the NPDR group ($P = 0.07$). Periodic shifts of velocity related to pulsation were observed in three groups (Fig. 6). Tendencies toward higher velocity during diastole and a lower velocity during systole were observed in all three groups ($P < 0.001$ for the normal group; $P = 0.003$, NDR group; and $P = 0.01$, NPDR group). The average PI was 0.44 ± 0.16 in the normal group, 0.43 ± 0.19 in the NDR group, and 0.46 ± 0.13 in the NPDR group. No significant differences in PI were detected among the groups ($P = 0.89$) (Fig. 5D).

Differences in the Erythrocyte Aggregate Elongation Rate

The elongation rates of 66 erythrocyte aggregates from 18 (90.0%) of 20 normal subjects, 45 erythrocyte aggregates from 12 (70.6%) of 17 patients with NDR, and 19 erythrocyte aggregates from 7 (70.0%) of 10 patients with NPDR were calculated successfully. The remaining subjects were excluded from the analysis of erythrocyte aggregate elongation because of the poor quality of the ST images. In these images, the bottom line of the erythrocyte aggregate corresponded to the

Investigative Ophthalmology & Visual Science

Downloaded From: http://iovs.arvojournals.org/pdfaccess.ashx?url=/data/Journals/IOVS/933678/ on 05/29/2015 Terms of Use:

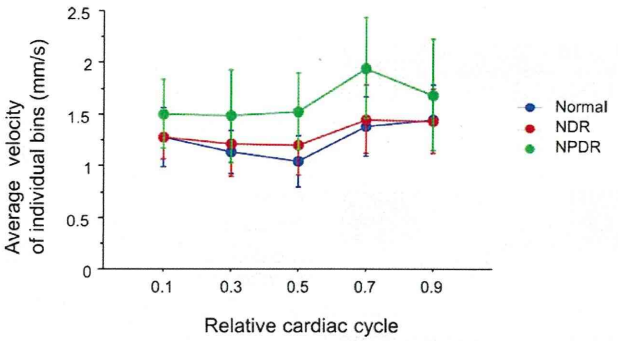

FIGURE 6. Pulsation of blood flow as detected in normal subjects, patients with NDR, and patients with NPDR. A relative cardiac cycle was assigned to each erythrocyte aggregate velocity in order to investigate the effect of cardiac pulsation on velocity. Velocity fluctuation was detected in a single relative cardiac cycle for all three groups. The maximum velocities tended to be observed in bins assigned to 0.7 or 0.9, which corresponded roughly to the diastolic phase. Meanwhile, minimum velocities were observed in the bin assigned to 0.5, which corresponded to the systolic phase. Statistical significances were found in the normal group ($P < 0.001$), in the NDR group ($P = 0.003$), and in the NPDR group ($P = 0.01$). The average pulsatility index values were 0.44 ± 0.16 in the normal group, 0.43 ± 0.19 in the NDR group, and 0.46 ± 0.13 in the NPDR group.

trajectory of the tail end of the erythrocyte aggregate and was not depicted clearly. The average elongation rates were 0.67 ± 0.20 in the normal group, 0.39 ± 0.19 in the NDR group, and 0.33 ± 0.11 in the NPDR group, respectively. Elongation rates in the NDR group ($P = 0.003$) and NPDR group ($P = 0.001$) were significantly lower than those in the normal group (Fig. 5E). However, there was no difference in elongation rate between the NDR group and the NPDR group ($P = 0.93$).

Categorization of Spatiotemporal Images

In total, 71 ST images from 18 (90%) normal subjects, 56 from 14 (82.4%) patients with NDR, and 36 from 7 (70.0%) patients with NPDR were used to categorize ST image type. The percentage of each type was as follows: 38.0% for type 1, 52.1% for type 2, 7.0% for type 3, and 2.8% for type 4 in the normal group; 16.1% for type 1, 42.9% for type 2, 25.0% for type 3, and 16.1% for type 4 in the NDR group; 13.9% for type 1, 30.6% for type 2, 30.6% for type 3, and 25.0% for type 4 in the NPDR group (Fig. 7). The NDR group and NPDR group had lower proportions of type 1 and type 2 and higher proportions of types 3 and 4 compared with the normal group.

Correlations Among Erythrocyte Aggregate Velocity, Elongation Rate, and HbA1c Level

In the NDR group, velocity had a tendency to correlate negatively with HbA1c levels, but the trend was not significant ($P = 0.09$, $r = -0.44$). No correlation was found between velocities and HbA1c levels in the NPDR group ($P = 0.73$, $r = 0.13$). A significant correlation was observed between the elongation rate and HbA1c negativity in the NDR group ($P = 0.002$, $r = -0.76$) and positivity in the NPDR group ($P = 0.02$, $r = 0.81$).

DISCUSSION

The aim of this study was to investigate hemorheologic properties in diabetic patients using AO-SLO, which allows for the direct and noninvasive visualization of retinal hemorheology in diabetic patients. Careful observation of the AO videos revealed that flow velocity fluctuations were found with higher frequency in diabetic patients than in normal subjects, suggesting that the hemorheologic changes in diabetic patients are captured accurately by AO videos. Although differences in erythrocyte aggregate velocity in the parafoveal network were found between normal subjects and NPDR patients, but not between normal subjects and NDR patients, erythrocyte aggregates in NDR patients who have no clinical appearance of retinopathy and NPDR patients showed lower elongation rates than those observed in normal subjects. Moreover, ST images that showed time-dependent changes in blood corpuscle arrangements and deformations could be categorized into four types. Differences in the proportion of each type of ST image were found between normal subjects and diabetic patients, suggesting that ST images can be used to visualize subclinical rheologic changes related to retinopathy in diabetic patients.

Retinal blood flow velocity changes associated with DM have long been investigated. In particular, the ability to measure velocity in NDR or early-stage DR has important implications for the early detection of retinopathy. However, the challenges inherent in these measurements have resulted in conflicting reports.[34,35] Considering only the results from research on human capillaries, it seems that blood flow velocity is decreased in diabetic patients.[34] To our knowledge, Tam et al.[34] published the first and only report on blood flow velocity in the retinal capillaries of diabetic patients as measured using AO-SLO. Their results showed that the velocities in seven type 2 diabetic patients with NDR were 14% lower than those of eight nondiabetic controls, but the trend lacked statistical significance. However, in this study, there was no significant difference in the overall average velocity of erythrocyte aggregates in the parafoveal capillary network between patients with NDR and nondiabetic controls, although retinal blood flow changes were reported as a primary reflection of retinal vascular endothelial dysfunction resulting from diabetes-related metabolic abnormalities.[36] One of the possible reasons for this difference in velocity could be the presence or absence of vessels with flow velocity fluctuations, which could lead to the measurement of extremely slow flow velocities. Because we excluded these vessels—which might represent leukostasis—from the analysis because of the difficulty in calculating accurate mean velocities, our results may have overestimated velocity in diabetic patients, as compared with other studies. Another potential reason for the discrepancy is that diabetic control statuses differ from study to study because retinal blood flow is modulated by glycemic control. Lorenzi et al.[37] reported that type 1 diabetic patients with no or minimal retinopathy who maintain relatively good glycemic control did not show abnormalities of the arterial retinal circulation as measured using laser Doppler flowmetry. Clermont and Bursell reported that there was a significant negative association between retinal blood flow and glycemic control.[36] Actually, in this study, the overall average velocities tended to correlate negatively with HbA1c levels in the NDR group; therefore, the distribution of diabetic control status may have affected our measurements of velocity in patients with NDR.

Calculating the velocity of moving objects in sequential video frames using ST images is a popular digital image-processing technique in the field of biomedical research.[38,39] In this study, we used ST images generated from capillary blood flow to map not only velocity but also the arrangements and deformations of blood corpuscles, which enabled us to visually understand the hemorheologic conditions in a given eye. The results showed differences in the types of ST images obtained

Investigative Ophthalmology & Visual Science

Downloaded From: http://iovs.arvojournals.org/pdfaccess.ashx?url=/data/Journals/IOVS/933678/ on 05/29/2015 Terms of Use:

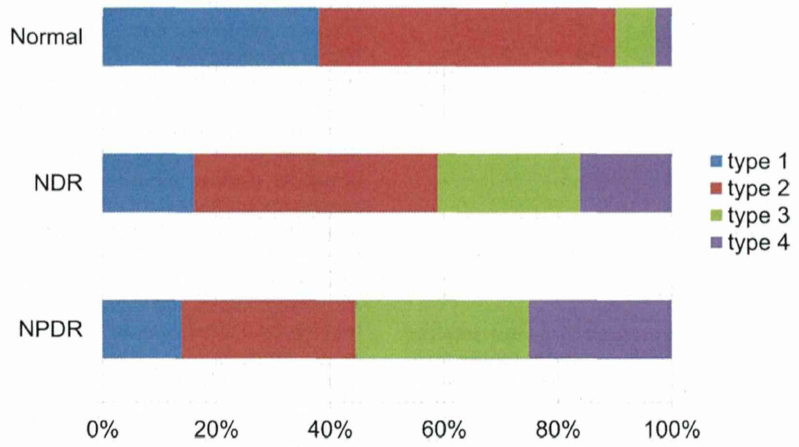

FIGURE 7. Histogram representing the ratio of ST image types in normal subjects, patients with NDR, and patients with NPDR. The NDR and NPDR groups had lower proportions of types 1 and 2 and much higher proportions of type 3 images, which represented minor changes in the elongation rate of erythrocyte aggregates, and type 4, which represented the presence of velocity changes in comparison with the normal group.

between normal subjects and diabetic patients. Type 1 and type 2 images, which represent the gradual elongation of erythrocyte aggregates, were more common in normal subjects, while type 3 images, which represented minor changes in elongation, and type 4, which represented flow velocity fluctuation, were seen only rarely. In contrast, diabetic patients had fewer type 1 and 2 images and more type 3 and 4 images when compared with normal subjects. Notably, types 3 and 4 accounted for more than 50% of the ST images obtained for NPDR patients. For further investigation, characteristics of the ST images, with the exception of type 4 ST images, were quantified by calculating the rate of erythrocyte aggregate elongation. Subsequent analyses verified that elongation rate was significantly lower in patients with NDR and NPDR as compared to normal subjects, and the erythrocyte aggregate elongation rates and HbA1c levels correlated significantly and negatively in the NDR group, suggesting that hemorheologic changes are apparent in AO-SLO videos before the clinical appearance of DR. Notably, one factor that can decrease the elongation rate of erythrocyte aggregates is the reduced deformability of erythrocytes in DM patients. Although erythrocytes can deform to pass through capillaries, the deformability of erythrocytes in patients with DM is reduced.[12,13] The reduced deformability of erythrocytes can prevent the cell from entering the capillary and consequently decrease the elongation rate in the microcirculation. Increased erythrocyte aggregability can also decrease the elongation rate in DM, perhaps by promoting the production of erythrocyte aggregates and the elongation of erythrocyte aggregates.[13] Taking into consideration that the total count of erythrocytes is limited, reduced numbers of isolated erythrocytes could also lead to a decrease in the elongation rate.

Significant changes in velocity and elongation rate were noted at different stages of DR. These results led us to speculate that vessel morphology might contribute to velocity changes, as changes in velocity occur after the clinical appearance of DR. The reduced elongation rate of erythrocyte aggregates could be considered to be a result of changes in deformability and aggregability. One potential reason for the differences in velocity between NDR and NPDR may be that leukocytes and erythrocyte aggregates have preferred pathways,[28,40] while neither cell type tends to pass through plasma gap capillaries (PGCs). As Tam et al.[21] theorized that leukocyte preferred paths (LPPs) might prevent leukocytes from entering non-LPP capillaries and PGCs may serve as relief valves to minimize flow disruption when a leukocyte enters a nearby LPP, PGCs may work to curb the increase in blood cell velocity in LPPs or erythrocyte aggregate preferred paths in NDR. Impaired flow through PGCs may increase the velocity of blood cells in nearby LPPs. Nonetheless, the impairment of LPPs or erythrocyte aggregate preferred pathways may force leukocytes or erythrocyte aggregates to enter PGCs, which may lead to intravascular stasis, in a vicious circle.

One limitation of this study was the relatively small sample size. Although significant correlation was observed between the elongation rate and HbA1c negativity in the NDR group and positivity in the NPDR group, it was difficult to interpret the reverse correlation. To achieve this, an appropriate sample size is required. An increase in the rate of successful image acquisition could be achieved by further developing the associated hardware and software, which in turn could enable larger studies in the future. Another limitation of this study is the lack of a longitudinal study, which is required to determine which patients will progress and which predictive value can be considered.

In conclusion, AO-SLO movies represent a noninvasive tool that provides hemorheologic information that can be used to measure the velocity and elongation rate of erythrocyte aggregates in patients with DM. Optics scanning laser ophthalmoscopy technology could shed light on investigations of the microcirculation in diabetic patients.

Acknowledgments

This study was presented in part at the Association for Research in Vision and Ophthalmology (ARVO) meeting in Orlando, Florida, in May 2014.

Supported, in part, by the Innovative Techno-Hub for Integrated Medical Bio-Imaging of the Project for Developing Innovation Systems, from the Ministry of Education, Culture, Sports, Science and Technology (MEXT) in Japan. The authors alone are responsible for the content and writing of the paper.

Disclosure: **S. Arichika**, None; **A. Uji**, None; **T. Murakami**, None; **N. Unoki**, None; **S. Yoshitake**, None; **Y. Dodo**, None; **S. Ooto**, None; **K. Miyamoto**, None; **N. Yoshimura**, Topcon Corporation (F), Nidek (F, C), Canon (F)

Downloaded From: http://iovs.arvojournals.org/pdfaccess.ashx?url=/data/Journals/IOVS/933678/ on 05/29/2015 Terms of Use:

References

1. Yau JW, Rogers SL, Kawasaki R, et al. Global prevalence and major risk factors of diabetic retinopathy. *Diabetes Care*. 2012; 35:556–564.
2. Kempen JH, O'Colmain BJ, Leske MC, et al. The prevalence of diabetic retinopathy among adults in the United States. *Arch Ophthalmol*. 2004;122:552–563.
3. The effect of intensive treatment of diabetes on the development and progression of long-term complications in insulin-dependent diabetes mellitus. The Diabetes Control and Complications Trial Research Group. *N Engl J Med*. 1993;329: 977–986.
4. Shichiri M, Kishikawa H, Ohkubo Y, Wake N. Long-term results of the Kumamoto Study on optimal diabetes control in type 2 diabetic patients. *Diabetes Care*. 2000;23(suppl 2):B21–29.
5. Kramer CK, Rodrigues TC, Canani LH, Gross JL, Azevedo MJ. Diabetic retinopathy predicts all-cause mortality and cardiovascular events in both type 1 and 2 diabetes: meta-analysis of observational studies. *Diabetes Care*. 2011;34:1238–1244.
6. Juutilainen A, Lehto S, Ronnemaa T, Pyorala K, Laakso M. Retinopathy predicts cardiovascular mortality in type 2 diabetic men and women. *Diabetes Care*. 2007;30:292–299.
7. Kawasaki R, Tanaka S, Abe S, et al. Risk of cardiovascular diseases is increased even with mild diabetic retinopathy: the Japan Diabetes Complications Study. *Ophthalmology*. 2013; 120:574–582.
8. Early Treatment Diabetic Retinopathy Study Research Group. Grading diabetic retinopathy from stereoscopic color fundus photographs—an extension of the modified Airlie House classification. ETDRS report number 10. *Ophthalmology*. 1991;98:786–806.
9. Curtis TM, Gardiner TA, Stitt AW. Microvascular lesions of diabetic retinopathy: clues towards understanding pathogenesis? *Eye (Lond)*. 2009;23:1496–1508.
10. Joussen AM, Murata T, Tsujikawa A, Kirchhof B, Bursell SE, Adamis AP. Leukocyte-mediated endothelial cell injury and death in the diabetic retina. *Am J Pathol*. 2001;158:147–152.
11. Miyamoto K, Ogura Y, Kenmochi S, Honda Y. Role of leukocytes in diabetic microcirculatory disturbances. *Microvasc Res*. 1997;54:43–48.
12. Singh M, Shin S. Changes in erythrocyte aggregation and deformability in diabetes mellitus: a brief review. *Indian J Exp Biol*. 2009;47:7–15.
13. Cho YI, Mooney MP, Cho DJ. Hemorheological disorders in diabetes mellitus. *J Diabetes Sci Technol*. 2008;2:1130–1138.
14. Babu N, Singh M. Analysis of aggregation parameters of erythrocytes in diabetes mellitus. *Clin Hemorheol Microcirc*. 2005;32:269–277.
15. Le Devehat C, Khodabandehlou T, Vimeux M. Impaired hemorheological properties in diabetic patients with lower limb arterial ischaemia. *Clin Hemorheol Microcirc*. 2001;25: 43–48.
16. Vinik AI, Erbas T, Park TS, Nolan R, Pittenger GL. Platelet dysfunction in type 2 diabetes. *Diabetes Care*. 2001;24:1476–1485.
17. Beutelspacher SC, Serbecic N, Barash H, et al. Retinal blood flow velocity measured by retinal function imaging in retinitis pigmentosa. *Graefes Arch Clin Exp Ophthalmol*. 2011;249: 1855–1858.
18. Nicolela MT, Hnik P, Drance SM. Scanning laser Doppler flowmeter study of retinal and optic disk blood flow in glaucomatous patients. *Am J Ophthalmol*. 1996;122:775–783.
19. Demiroglu H. The importance of erythrocyte aggregation in blood rheology: considerations on the pathophysiology of thrombotic disorders. *Blood*. 1997;89:4236.
20. Roorda A, Williams DR. The arrangement of the three cone classes in the living human eye. *Nature*. 1999;397:520–522.
21. Tam J, Tiruveedhula P, Roorda A. Characterization of single-file flow through human retinal parafoveal capillaries using an adaptive optics scanning laser ophthalmoscope. *Biomed Opt Express*. 2011;2:781–793.
22. Martin JA, Roorda A. Pulsatility of parafoveal capillary leukocytes. *Exp Eye Res*. 2009;88:356–360.
23. Uji A, Hangai M, Ooto S, et al. The source of moving particles in parafoveal capillaries detected by adaptive optics scanning laser ophthalmoscopy. *Invest Ophthalmol Vis Sci*. 2012;53: 171–178.
24. Arichika S, Uji A, Hangai M, Ooto S, Yoshimura N. Noninvasive and direct monitoring of erythrocyte aggregates in human retinal microvasculature using adaptive optics scanning laser ophthalmoscopy. *Invest Ophthalmol Vis Sci*. 2013;54:4394–4402.
25. Tam J, Martin JA, Roorda A. Noninvasive visualization and analysis of parafoveal capillaries in humans. *Invest Ophthalmol Vis Sci*. 2010;51:1691–1698.
26. Chui TY, Gast TJ, Burns SA. Imaging of vascular wall fine structure in the human retina using adaptive optics scanning laser ophthalmoscopy. *Invest Ophthalmol Vis Sci*. 2013;54: 7115–7124.
27. Takayama K, Ooto S, Hangai M, et al. High-resolution imaging of the retinal nerve fiber layer in normal eyes using adaptive optics scanning laser ophthalmoscopy. *PLoS One*. 2012;7: e33158.
28. Arichika S, Uji A, Ooto S, Miyamoto K, Yoshimura N. Adaptive optics-assisted identification of preferential erythrocyte aggregate pathways in the human retinal microvasculature. *PLoS One*. 2014;9:e89679.
29. Ogura Y. In vivo evaluation of leukocyte dynamics in the retinal and choroidal circulation. *Jpn J Ophthalmol*. 2000;44: 322–323.
30. Wilkinson CP, Ferris FL III, Klein RE, et al. Proposed international clinical diabetic retinopathy and diabetic macular edema disease severity scales. *Ophthalmology*. 2003;110: 1677–1682.
31. Hirose FNK, Saito K, Numajiri Y. A compact adaptive optics scanning laser ophthalmoscope with high-efficiency wavefront correction using dual liquid crystal on silicon—spatial light modulator. In: Manns F, Söderberg P, Ho A, eds. *Proceedings of SPIE*. Vol. 7885. SPIE.Digital Library; 2011. DOI:10.1117/12.873671.
32. Lasers ANSftSUo. American National Standard for the Safe Use of Lasers. American National Standards Institute. ANSIZ136. New York, NY: American National Standards Institute; 2007.
33. Bennett AG, Rudnicka AR, Edgar DF. Improvements on Littmann's method of determining the size of retinal features by fundus photography. *Graefes Arch Clin Exp Ophthalmol*. 1994;232:361–367.
34. Tam J, Dhamdhere KP, Tiruveedhula P, et al. Disruption of the retinal parafoveal capillary network in type 2 diabetes before the onset of diabetic retinopathy. *Invest Ophthalmol Vis Sci*. 2011;52:9257–9266.
35. Nagaoka T, Sato E, Takahashi A, Yokota H, Sogawa K, Yoshida A. Impaired retinal circulation in patients with type 2 diabetes mellitus: retinal laser Doppler velocimetry study. *Invest Ophthalmol Vis Sci*. 2010;51:6729–6734.
36. Clermont AC, Bursell SE. Retinal blood flow in diabetes. *Microcirculation*. 2007;14:49–61.
37. Lorenzi M, Feke GT, Cagliero E, et al. Retinal haemodynamics in individuals with well-controlled type 1 diabetes. *Diabetologia*. 2008;51:361–364.

Investigative Ophthalmology & Visual Science

Downloaded From: http://iovs.arvojournals.org/pdfaccess.ashx?url=/data/Journals/IOVS/933678/ on 05/29/2015 Terms of Use:

38. Sato Y, Chen J, Zoroofi RA, Harada N, Tamura S, Shiga T. Automatic extraction and measurement of leukocyte motion in microvessels using spatiotemporal image analysis. *IEEE Trans Biomed Eng*. 1997;44:225–236.
39. Mostany R, Chowdhury TG, Johnston DG, Portonovo SA, Carmichael ST, Portera-Cailliau C. Local hemodynamics dictate long-term dendritic plasticity in peri-infarct cortex. *J Neurosci*. 2010;30:14116–14126.
40. Nishiwaki H, Ogura Y, Kimura H, Kiryu J, Miyamoto K, Matsuda N. Visualization and quantitative analysis of leukocyte dynamics in retinal microcirculation of rats. *Invest Ophthalmol Vis Sci*. 1996;37:1341–1347.

Investigative Ophthalmology & Visual Science

Downloaded From: http://iovs.arvojournals.org/pdfaccess.ashx?url=/data/Journals/IOVS/933678/ on 05/29/2015 Terms of Use:

Parallelism for Quantitative Image Analysis of Photoreceptor–Retinal Pigment Epithelium Complex Alterations in Diabetic Macular Edema

Akihito Uji, Tomoaki Murakami, Noriyuki Unoki, Ken Ogino, Takahiro Horii, Shin Yoshitake, Yoko Dodo, and Nagahisa Yoshimura

Department of Ophthalmology and Visual Sciences, Kyoto University Graduate School of Medicine, Kyoto, Japan

Correspondence: Akihito Uji, Department of Ophthalmology and Visual Sciences, Kyoto University Graduate School of Medicine, 54 Shogoin Kawahara-cho, Sakyo-ku, Kyoto 606-8507, Japan; akihito1@kuhp.kyoto-u.ac.jp.

Submitted: January 13, 2014
Accepted: April 27, 2014

Citation: Uji A, Murakami T, Unoki N, et al. Parallelism for quantitative image analysis of photoreceptor-retinal pigment epithelium complex alterations in diabetic macular edema. *Invest Ophthalmol Vis Sci.* 2014;55:3361-3367. DOI:10.1167/iovs.14-13948

Purpose. To propose a new method to quantitatively and comprehensively evaluate photoreceptor-RPE complex alterations on spectral-domain optical coherence tomography (SD-OCT) imaging in eyes with diabetic macular edema (DME).

Methods. Spectral-domain OCT images from a consecutive series of 90 eyes in 79 patients with DME and 30 healthy eyes in 30 volunteers were analyzed retrospectively. The subfoveal area covering the photoreceptor layers was skeletonized and the orientation of the segmented lines was termed "parallelism," which reflects image complexity. Photoreceptor layer status at the fovea was categorized by graders, including continuity of the external limiting membrane (ELM) line, inner segment ellipsoid line, and the presence of hyperreflective foci in the outer retinal layers. The relationships among parallelism, visual acuity, and photoreceptor layer status were evaluated.

Results. Parallelism was significantly lower in eyes with DME than in normal eyes ($P < 0.0001$), and correlated strongly with visual acuity in eyes with DME ($R = -0.592$; $P < 0.0001$). Eyes with an intact inner segment ellipsoid line or ELM line had significantly better visual acuity (VA) and higher parallelism than eyes with a discontinuous or absent inner segment ellipsoid line or ELM line. Parallelism was significantly higher ($P < 0.0001$) and logMAR VA significantly better ($P < 0.0001$) in the group without hyperreflective foci in the outer retinal layers than in the group with hyperreflective foci in the outer retinal layers.

Conclusions. Parallelism has the potential to reflect structural changes of the photoreceptor layers in DME.

Keywords: diabetic macular edema, optical coherence tomography, image analysis

Diabetic macular edema (DME) is a leading cause of visual dysfunction in patients with diabetes. The number of patients with diabetic retinopathy is expected to increase over the next few decades; therefore, a further revitalization of research and development on efficient and high-quality evaluation techniques for DME needs to be addressed.[1,2]

Along with the popularization of optical coherence tomography (OCT) in recent decades, clinicians have been able to detect thickening of the sensory retina and vascular lesions in DME more easily and objectively compared with examination using biomicroscopy only.[3–5] In particular, OCT has enabled clinicians to objectively measure retinal thickness for assessments of disease severity or therapy evaluations, and a modest correlation between OCT-measured central retinal thickness and visual acuity (VA) has been reported in DME to date.[4–10]

More recently, because of improvements in OCT image quality achieved by developments in both hardware and software, later generations of OCT systems have provided cross-sectional imaging of the retina at a higher resolution, allowing clinicians to analyze smaller structures and the individual retinal layers.[11–14] In particular, the external limiting membrane (ELM), which corresponds to the adherens junctions between the Müller cells and photoreceptor cells,[15] and the inner segment ellipsoid line[16] on the OCT images reportedly provide important information about pathologies of the photoreceptors.[17–20] Hyperreflective foci in DME, subclinical findings that are invisible during clinical ophthalmoscopic examinations, are related to foveal photoreceptor damage and concomitant visual disturbance.[21–24] A correlation has been established between damage to the foveal photoreceptors and the VA in retinal diseases, including DME, suggesting the clinical relevance of both macular thickening and the photoreceptor damage in DME.[25]

Several methods, including detection of inner segment ellipsoid line and ELM discontinuities or measurement of photoreceptor outer segment (PROS) lengths, have been reported for qualitative or quantitative evaluations of the photoreceptor layer on OCT images by using graders or software.[18–20,26–28] However, alterations of the photoreceptor layer on OCT images of eyes with DME involve not only discontinuities of the inner segment ellipsoid lines and ELM lines, but also transformations of these lines, the presence of hyperreflective foci, and irregular RPE lines; these features are too complicated to evaluate by looking at only one aspect of the alterations.[22,23,29] The development of robust algorithms for comprehensive analyses are eagerly anticipated.

Copyright 2014 The Association for Research in Vision and Ophthalmology, Inc.

Downloaded From: http://iovs.arvojournals.org/pdfaccess.ashx?url=/data/Journals/IOVS/932989/ on 05/29/2015 Terms of Use:

In this study, we proposed a new method to quantitatively and comprehensively evaluate the complexity of photoreceptor-RPE complex alterations by using "parallelism," which we previously reported as a new, robust, and practical parameter of the structural integrity of retinal layers.[30] This parameter reflects how parallel line objects are to each other on OCT images and can be calculated using line segments generated by simply filtering and thresholding the original image. The increased complexity of photoreceptor-RPE complex images as a result of the above-mentioned alterations in DME has the potential to decrease parallelism. The algorithm for calculating parallelism was tested using OCT scans from healthy subjects and patients with DME, and its clinical relevance was explored.

Methods

Subjects

This was a retrospective, observational, cross-sectional study. All the research and measurements adhered to the tenets of the Declaration of Helsinki and were approved by the institutional review board at Kyoto University Graduate School of Medicine for retrospective review of existing patient data. We retrospectively examined 90 eyes in 79 patients (mean age ± SD, 65.3 ± 8.6 years; range, 35–88 years) with DME who visited Kyoto University Hospital from June 2008 through June 2010. The inclusion criterion was the availability of spectral domain OCT (SD-OCT) images of sufficient quality. All patients had undergone comprehensive ophthalmologic examinations, including measurements of best-corrected VA (BCVA), slit-lamp biomicroscopy, color fundus photography, and SD-OCT. The exclusion criteria included the presence of serous retinal detachment, hard exudates at the fovea, significant media opacities (including cataract or vitreous hemorrhage), and other retinal diseases, such as uveitis or vitreomacular traction syndrome. Data for 30 eyes of 30 volunteers (63.0 ± 9.9 years; range, 38–77 years) were retrospectively collected from our database of healthy volunteers as candidate control eyes.

Optical Coherence Tomography

Spectral-domain OCT (Spectralis; Heidelberg Engineering, Heidelberg, Germany) images were used for analyses of retinal sectional images of the macula. Sixty-one raster scans (30 × 25 degrees) in high-speed mode and 30-degree cross-hair scans in high-resolution mode were used in this study. Raster scans were used for mean foveal thickness measurement (radius, 500 μm) using built-in software, and cross-sectional images were used for calculation of parallelism. The presumed foveal center was determined as the area lacking inner retinal layers in the macular region[31] and the pathomorphology within a 1-mm area centered at the presumed fovea was assessed for each eye. We evaluated the status of the ELM line, inner segment ellipsoid line at the fovea, and the presence of hyperreflective foci in the outer retinal layers, as previously described.[22] Eyes in which the inner segment ellipsoid line was detected as a complete line in the fovea were classified as inner segment ellipsoid line(+), and eyes in which the inner segment ellipsoid line was detected as a discontinuous line in the fovea were classified as inner segment ellipsoid line(±); when the inner segment ellipsoid line could not be detected in the fovea, eyes were classified as inner segment ellipsoid line(–). Each eye also was classified based on the status of the ELM line beneath the fovea by using the same criteria described for the inner segment ellipsoid line (i.e., ELM line[+], ELM line[±], and ELM line[–]). Two experienced examiners (KO, TH) blinded to the clinical findings categorized the status of the outer retinal layers, including continuity of the inner segment ellipsoid line, continuity of the ELM line, and the presence of hyperreflective foci. In cases of disagreement, the results were discussed until consensus was reached. The kappa coefficient was calculated as a measure of agreement between the observers.

Calculation of Parallelism

Cross-sectional images at 30 degrees through the fovea were chosen for each eye. To quantitatively evaluate the complexity of photoreceptor-RPE complex alterations, we first cropped a rectangular region of interest (ROI) measuring 1000 × 150 μm covering the photoreceptor-RPE complex at the fovea, and extracted skeletonized images (lines) from the OCT images by applying filtration through a 1- to 2-pixel band-pass filter using an ImageJ (http://imagej.nih.gov/ij/; provided in the public domain by the National Institutes of Health, Bethesda, MD, USA) software plug-in Kbi_BandPass (http://hasezawa.ib.k.u-tokyo.ac.jp/zp/Kbi/ImageJKbiPlugins) followed by binarization with intensity thresholding using Otsu's thresholding method for automatic binarization-level decisions using the plug-in Kbi_ThrOtsu (http://hasezawa.ib.k.u-tokyo.ac.jp/zp/Kbi/ImageJKbiPlugins) (Fig. 1).[32–34] It is of note that the analysis of parallelism requires only information regarding the orientation of structures in the ROI, which can be obtained using line segments rather than solid lines. The calculation of parallelism from the skeletonized image was fully described in previous articles.[30,32,33] Briefly, in digital images, neighboring pixel pairs can be categorized as 0°, 45°, 90°, and 135° with respect to the horizon. In this study, parallelism was defined as follows:

$$\text{Parallelism} = \frac{|n_0 - n_{90}| + |n_{45} - n_{135}|}{n_0 + n_{45} + n_{90} + n_{135}}, \qquad (1)$$

where n_0, n_{45}, n_{90}, and n_{135} are the numbers of pixel pairs at 0°, 45°, 90°, and 135°, respectively. Parallelism can range from 0 to 1, and images with more parallel line segments have higher parallelism. The mean parallelism values from a horizontal scan and vertical scan were calculated for each eye and used for the analyses. All digital images were processed by a single operator (AU) using ImageJ and a software plug-in.

Statistical Analysis

All values are expressed as mean ± SD. All BCVA measurements were converted to logMAR equivalents before statistical analysis. Comparisons between healthy subjects and DME patients with regard to age, logMAR VA, parallelism, and retinal thickness were performed using Student's *t*-tests. Comparisons of the logMAR VA values and parallelism of the three groups classified based on the status of the inner segment ellipsoid line or ELM line were carried out using a one-way ANOVA, with post hoc comparisons tested by the Scheffé procedure. Comparisons of the logMAR VA values and parallelism between the two hyperreflective foci groups (foci absent in the outer retinal layers group versus foci present in the outer retinal layers group) were carried out using Student's *t*-tests. The relationships between logMAR VA and parallelism, logMAR VA and foveal thickness, and parallelism and foveal thickness were analyzed using Pearson's correlation coefficient. A P value less than 0.05 was considered statistically significant. All analyses, except for the kappa coefficient assessments, were performed using StatView (version 5.0; SAS Institute, Cary, NC, USA). Calculation of the kappa coefficient was performed using SPSS (version 17; SPSS Inc., Chicago, IL, USA).

Investigative Ophthalmology & Visual Science

Downloaded From: http://iovs.arvojournals.org/pdfaccess.ashx?url=/data/Journals/IOVS/932989/ on 05/29/2015 Terms of Use:

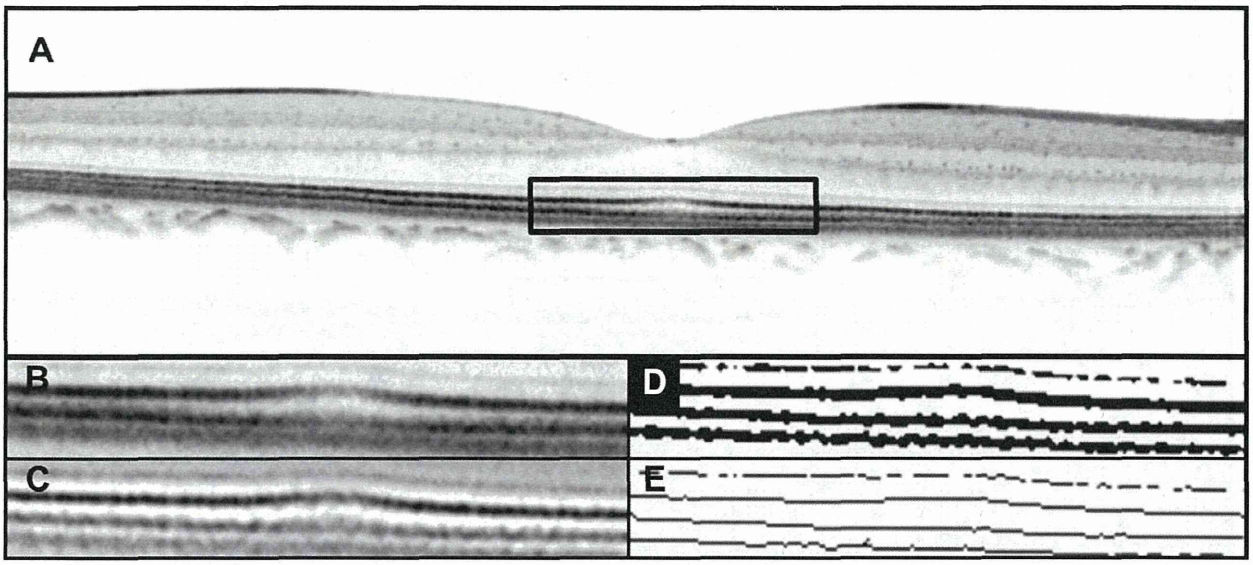

FIGURE 1. Calculation of parallelism through skeletonizing OCT images of the photoreceptor-RPE complex in a healthy subject. Images are of the right eye of a 74-year-old woman from our database of healthy volunteers. (**A**) A horizontal line scan from an SD-OCT image. (**B**) A magnified view of the area *outlined in black* in (**A**). (**C**) A filtered image of (**B**) after the application of a band-pass filter for noise reduction and enhancement of the line segments. (**D**) A binarized image of (**C**) after using Otsu's thresholding method for automatic binarization level decisions. (**E**) A skeletonized image generated from (**D**). Each line segment represents the orientation of the striped pattern of the photoreceptor-RPE complex. Line segments are depicted as parallel lines, and the parallelism calculated for this area was 0.937.

RESULTS

Assessment of Interobserver Agreement

The kappa coefficient was 0.704 ($P < 0.001$) for the ELM line, 0.809 ($P < 0.001$) for the inner segment ellipsoid line, and 0.756 ($P < 0.001$) for the presence of hyperreflective foci. The results indicated good interobserver agreement.

Differences in Parallelism Between Healthy Subjects and Patients With DME

Skeletonized OCT images in cases of DME with disrupted ELM or inner segment ellipsoid lines and hyperreflective foci in the outer retinal layers showed many line segments in random orientations in the ROI, which have the potential to decrease the parallelism of the images (Fig. 2). Meanwhile, in healthy subjects and cases of DME with less disrupted photoreceptor layers and without hyperreflective foci in the outer retinal layers, line segments were observed as parallel lines (Figs. 1 and 3). Parallelism was significantly ($P < 0.0001$) lower and logMAR VA was significantly ($P < 0.0001$) worse in eyes with DME than in normal eyes (Table 1). Retinal thicknesses were significantly higher in eyes with DME than in normal eyes ($P < 0.0001$).

Association Between Parallelism and Photoreceptor Status

We further investigated how photoreceptor status in DME contributed to parallelism values. There were significant differences among the three inner segment ellipsoid line groups in parallelism ($P < 0.0001$) and logMAR VA ($P < 0.0001$) (Table 2). In the inner segment ellipsoid line(+) group, parallelism was significantly higher and logMAR VA was significantly better than those in either the inner segment ellipsoid line(±) ($P = 0.0077$ and $P = 0.0198$) or inner segment ellipsoid line(−) groups ($P < 0.0001$ for both comparisons). There also were significant differences among the three ELM line groups in parallelism ($P < 0.0001$) and logMAR VA ($P < 0.0001$). In the ELM line(+) group, parallelism was significantly higher and logMAR VA was significantly better than those in either the ELM line(±) ($P < 0.0001$ and $P = 0.0004$) or ELM line(−) groups ($P < 0.0001$ for both comparisons). Parallelism was significantly higher ($P < 0.0001$) and logMAR VA was significantly better in the group without hyperreflective foci in the outer retinal layers than in the group with hyperreflective foci in the outer retinal layers.

Correlation Among VA, Parallelism, and Foveal Thickness in Patients With DME

Parallelism correlated well with logMAR VA ($R = -0.592$; $P < 0.0001$) (Fig. 4). Moreover, foveal thickness correlated significantly with logMAR VA ($R = 0.381$; $P = 0.0002$). Significant negative correlations were observed between parallelism and foveal thickness ($R = -0.316$; $P = 0.0316$).

DISCUSSION

This study is based on a methodology according to which photoreceptor-RPE complex alterations in DME are comprehensively quantifiable by interpreting the alterations as changes in image complexity. Parallelism, a parameter reflecting the orientations of lines in the image, was applied as a parameter representing the complexity of photoreceptor-RPE complex alterations, and the results demonstrated that parallelism was clinically relevant in eyes with DME. To the best of our knowledge, this is the first study that used parallelism as a surrogate marker for photoreceptor-RPE complex alterations in OCT image analysis.

Significant differences between normal eyes and eyes with DME and significant correlations with VA were detected with the use of parallelism. Moreover, eyes with an intact inner segment ellipsoid line or ELM line had significantly higher

Investigative Ophthalmology & Visual Science

Downloaded From: http://iovs.arvojournals.org/pdfaccess.ashx?url=/data/Journals/IOVS/932989/ on 05/29/2015 Terms of Use: